Adsorption (2013) 19:1165–1180
DOI 10.1007/s10450-013-9546-z

Capacity and kinetic measurements of methane and nitrogen adsorption on H^+-mordenite at 243–303 K and pressures to 900 kPa using a dynamic column breakthrough apparatus

Thomas L. H. Saleman · Guillaume C. Y. Watson · Thomas E. Rufford · Paul S. Hofman · K. Ida Chan · Eric F. May

Received: 2 October 2012 / Accepted: 23 April 2013 / Published online: 5 May 2013

Abstract A dynamic column breakthrough (DCB) apparatus was used to measure the capacity and kinetics of CH_4 and N_2 adsorption on zeolite H^+-mordenite at temperatures in the range 243.8–302.9 K and pressures up to 903 kPa. Equilibrium adsorption capacities of pure CH_4 and pure N_2 were determined by these dynamic experiments and Langmuir isotherm models were regressed to these pure fluid data over the ranges of temperature and pressure measured. A linear driving force-based model of adsorption in a fixed bed was developed to extract the mass transfer coefficients (MTCs) for CH_4 and N_2 from the pure gas experimental data. The MTCs determined from single adsorbate experiments were used to successfully predict the component breakthroughs for experiments with equimolar $CH_4 + N_2$ gas mixtures in the DCB apparatus. The MTC of CH_4 on H^+-mordenite at 902 kPa was 0.013 s^{-1} at 302.9 K and 0.004 s^{-1} at 243.6 K. The MTC of N_2 on H^+-mordenite at 902 kPa was 0.011 s^{-1} at 302.9 K and 0.005 s^{-1} at 243.5 K. The values of the MTCs measured for each gas at a constant feed gas flow rate were observed to increase in a linear trend with the inverse of pressure. However, the apparent MTCs obtained at the lowest pressures studied ($\approx$105 kPa) were systematically below this linear trend, because of the slightly longer residence time of helium in the mass spectrometer used to monitor effluent composition. Nevertheless, the pure fluid dynamic breakthrough data at these lowest pressures could still be reasonably well described using MTC values estimated from the linear trend. Furthermore, the results of dynamic breakthrough experiments with mixtures were all reliably predicted using the capacity and MTC correlations developed for the pure fluids.

Keywords Zeolite · Pressure swing adsorption · Mass transfer coefficient · Linear driving force model · Langmuir isotherm · Natural gas

1 Introduction

The separation of nitrogen from methane is one of the most challenging gas processing operations in the production of liquefied natural gas (LNG). There are significant volumes of natural gas which are considered sub-quality due to their high concentrations of N_2, including about 16 trillion standard cubic feet of known gas reserves in the USA which contain more than 4 % N_2 (Baker 2002). Nitrogen has no useful heating value and thus the main driver for N_2 removal from gas destined for pipeline sales is to meet a specified minimum heating value of the gas. A typical gas pipeline specification for N_2 is 3 % (Kidnay and Parrish 2006) and in many cases the feed gas may meet this specification without need for nitrogen removal or it may be achieved for gas from a high N_2 content field by blending it with gas from a richer field. However, for LNG a maximum concentration of 1 % N_2 is often specified and, to achieve this specification, cryogenic distillation processes known industrially as Nitrogen Rejection Units (NRU) may be required. These cryogenic columns are both expensive and energy intensive and can add significantly to

T. L. H. Saleman · G. C. Y. Watson · T. E. Rufford · P. S. Hofman · E. F. May (✉)
Centre for Energy, School of Mechanical and Chemical Engineering, The University of Western Australia, 35 Stirling Highway, Crawley, WA 6009, Australia
e-mail: Eric.May@uwa.edu.au

K. I. Chan
Chevron Energy Technology Company, Houston, TX 77002, USA

gas production costs. An alternative technology that may have potential in such N_2 rejection processes is pressure swing adsorption (PSA); several such processes are already operated in the natural gas industry which use various adsorbents including activated carbons (American Energies Pipeline, LLC 2011) and titanosilicates (Mitariten 2009; Kuznicki et al. 1999). Carbon molecular sieves (Cavenati et al. 2006) and small-pore zeolites such as clinoptilolites (Jayaraman et al. 2004) have also been studied for their potential as N_2 selective adsorbents.

The design of PSA processes requires an accurate knowledge of the adsorption equilibria, kinetics and heats of adsorption for the gas mixture and the adsorbent at the conditions representative of the industrial process (Sircar 2006), which include the expected operating ranges of temperature, pressure and gas composition. While several experimental techniques can be used to measure the necessary sorption data, doing so with the dynamic column breakthrough (DCB) method has several advantages (Malek and Farooq 1996; Guntuka et al. 2008; Delgado et al. 2006b; Casas et al. 2012; Mulgundmath et al. 2012). Laboratory experiments made with the DCB method can more closely match the conditions in an industrial-scale fixed-bed gas separation process than achievable with static volumetric or gravimetric adsorption experiments (Rajendran et al. 2008). Furthermore, an appropriately instrumented DCB apparatus together with a mathematical model of the adsorption column can be used to determine equilibrium capacities as well as heat and mass transfer parameters from a single set of experiments (Puértolas et al. 2012). Many of the DCB experiments reported in the literature involve the injection of a dilute adsorbate within an inert carrier gas into the column packed with the adsorbent; such conditions simplify the material balance on the adsorbent bed because the effluent flow rate from the column does not vary significantly when the adsorbate concentration is dilute. In our previous paper (Hofman et al. 2012), we described the use of a DCB apparatus equipped with an accurate effluent flow meter to determine the equilibrium adsorption capacities, and their experimental uncertainty, from breakthrough experiments involving concentrated adsorbate feeds.

In this paper we apply a linear driving force (LDF)-based model of adsorption in a fixed bed to extract the mass transfer coefficients (MTCs) for CH_4 and N_2 on H^+-mordenite from pure fluid DCB experiments at temperatures in the range 243.8–302.9 K and pressures up to 903 kPa. Importantly, we provide a quantitative assessment of the uncertainty in these kinetic parameters plus we investigated the effects of temperature and pressure on the kinetics of both CH_4 and N_2. The equilibrium capacities measured with the DCB at these conditions are compared with adsorption isotherms measured on static volumetric apparatus previously in our laboratory (Jensen et al. 2012) and also by Delgado et al. (2006a). To validate the dynamic adsorption model as a tool to predict the separation of gas mixtures, the measured breakthrough curves from DCB experiments with feeds of $CH_4 + N_2$ mixtures are compared with the results of simulations made using the kinetic parameters extracted from the pure fluid measurements. In future work, such a dynamic adsorption model will be used to design and evaluate PSA processes for the separation of streams containing CH_4 and N_2 in natural gas processing plants.

2 Method and equilibrium analysis

A commercial zeolite H^+-mordenite (HSZ-640HOA from TOSOH Corporation, Japan) in the form of 1 mm diameter extruded pellets with an average length of 4 mm was studied in these experiments. Our laboratory previously characterized this adsorbent using N_2 sorption analyses at 77 K (Micromeritics ASAP2020) and measured a BET specific surface area of 363 $m^2\ g^{-1}$, a total pore volume of 0.340 $cm^3\ g^{-1}$ and a HK micropore volume of 0.174 $cm^3\ g^{-1}$ (Jensen et al. 2012). The skeletal density of the mordenite measured with a Helium pycnometer (Micromeritics AccuPyc 1330) was 2.5356 g cm^{-3}, and this parameter was used in the dynamic model.

All gases used in this work were supplied by BOC who stated the flowing fractional purities: He 99.999 %, CH_4 99.995 %, and N_2 99.999 %. The estimated uncertainty of the adsorption measurements due to the gas purity was assumed to be negligible.

The dynamic adsorption experiments were conducted with the DCB apparatus shown in Fig. 1. Details on the construction and operation of this apparatus, including descriptions of the instruments used for pressure, temperature, flow and gas composition measurements, were provided by Hofman et al. (2012). In that work, we also detailed a method of measuring the flow of effluent mixtures accurately during DCB experiments with concentrated adsorbates. The only significant modification made to the DCB apparatus for this work was the replacement of the stirred air bath with a circulating water-glycol bath. Submerging the adsorption column in the water–glycol bath provided better temperature control in the range 243–353 K and increased the rate of heat transfer from the column in comparison with the air bath. The increased rate of heat transfer meant that heat of adsorption effects were more rapidly dissipated, which in turn provided better experimental control.

Prior to loading into the adsorption column, the H^+-mordenite was regenerated in a separate vessel under a vacuum of 10 Pa at 573 K for 24 h, after which the

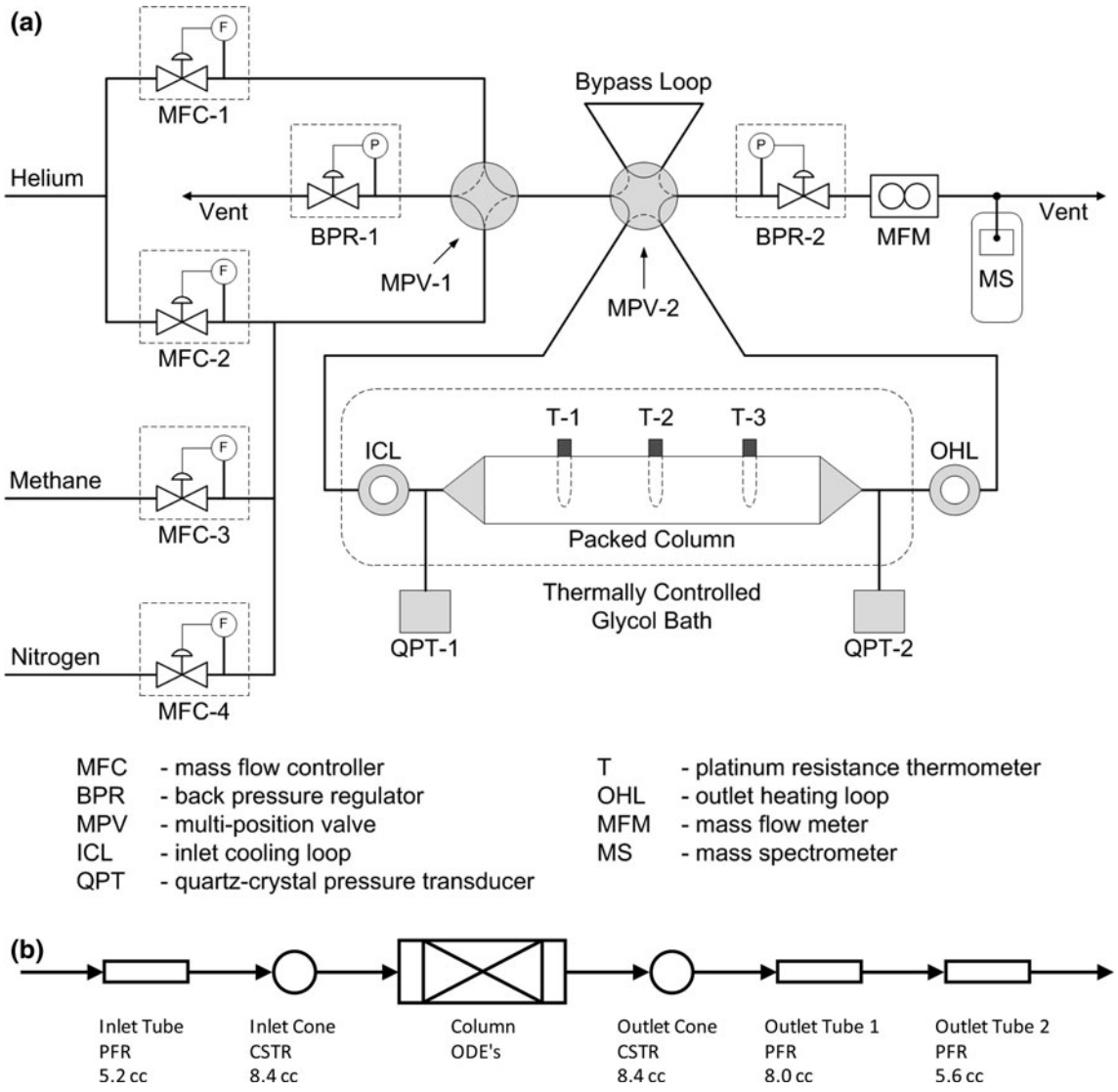

Fig. 1 Diagram of the DCB apparatus. **a** Process flow schematic of the DCB apparatus. Three thermometers were inserted along the length of the column at 32.7, 65.4 and 98.1 mm from the column entrance. The effluent gas flow rate from the column was measured with an orifice type flow meter corrected for the gas composition measured using a mass spectrometer. **b** Schematic layout of the DCB model. The tubes are represented by ideal PFRs and the cones are modeled as a single ideal CSTR. The packed adsorption column is a stainless steel tube (130 mm long and 22.2 mm internal diameter) and is modeled by a set of ordinary differential equations (ODEs)

regeneration vessel was backfilled with N_2. Loading of the regenerated adsorbent into the column was done as quickly as possible to minimize the exposure of the (N_2-saturated) H^+-mordenite to the air. The masses of the regenerated adsorbent used in two sets of DCB measurements were 30.252 ± 0.005 g and 29.669 ± 0.005 g. Once installed in the DCB apparatus the adsorbent was degassed in situ at 302 K in a 136 μmol s^{-1} helium flow for a minimum of 3 h. The effectiveness of this regeneration procedure was checked by repeating the 100 and 900 kPa runs at 303 and 243 K, with no inconsistencies observed.

Experiments with single adsorbates (CH_4, N_2) and with $CH_4 + N_2$ mixtures were conducted at temperatures in the range 243.7–302.9 K and total pressures from 103.8 to 902.8 kPa with the feed gas flow rate maintained at 68.1 μmol s^{-1} (100 standard cm^3 per minute). The adsorption of helium on zeolites such as H^+-mordenite can be assumed to be negligible at these experimental conditions (Malbrunot et al. 1997). As discussed by Hofman et al. (2012), this assumption was validated by a performing a consistency check between the measured volume of helium displaced from the column during DCB with the estimated total system void volume.

The measured excess adsorption capacities Q^*_{ex,CH_4} and Q^*_{ex,N_2}, along with the absolute adsorption capacities, for

the pure fluid experiments are listed in Table 1 for CH_4 and Table 2 for N_2. (The DCB method measures excess adsorption capacities because the volume of helium displaced from the column is assumed to be the same as the volume of gas in equilibrium with the adsorbed phase at the end of the experiment. However this neglects the volume of the adsorbed phase, which is not present when the column is filled with helium, and thus the DCB technique strictly measures excess capacities.) The absolute adsorption capacities were calculated from the measured excess capacities using an ideal mixing rule and literature estimates of adsorbed phase densities for pure compounds ($\rho_{ads,CH_4} = 0.354$ g cm^{-3} and $\rho_{ads,N_2} = 0.701$ g cm^{-3}) (Sudibandriyo et al. 2003; Watson et al. 2009). The molar density of the gas mixture was determined at the measured pressure, temperature and composition, from the GERG-2004 equation of state (Kunz et al. 2006) as implemented in the software REFPROP 8.0 (Lemmon et al. 2007). At the measurement conditions in this study the difference between absolute and excess adsorption capacities was small with $\left|Q^*_{abs,i} - Q^*_{ex,i}\right| / Q^*_{ex,i} \leq 0.02$. This is smaller than the relative uncertainties of the measured adsorption capacities, which had a minimum value of 0.04, as indicated in Tables 1 and 2.

The absolute adsorption capacity data for CH_4 and N_2 measured in the single pure fluid DCB experiments, were combined with the adsorption data reported by Jensen et al. (2012) and Hofman et al. (2012), and used in a

Table 1 Equilibrium excess (Q^*_{ex,CH_4}) and absolute (Q^*_{abs,CH_4}) adsorption capacities of CH_4 on H^+-mordenite measured on the DCB apparatus at a feed flow rate of 68.1 μmol s^{-1} of pure CH_4. The uncertainty $u(Q^*_{ex,CH_4})$ (mmol g^{-1}) in the adsorption capacity measurement is also reported

Methane				
P (kPa)	T (K)	Q^*_{ex,CH_4} (mmol g^{-1})	$u(Q^*_{ex,CH_4})$ (mmol g^{-1})	Q^*_{abs,CH_4} (mmol g^{-1})
104.9	302.9	0.490	0.025	0.491
105.6	302.8	0.514	0.026	0.515
105.6	302.9	0.516	0.026	0.517
106.7	302.8	0.498	0.026	0.499
153.0	302.9	0.666	0.030	0.668
207.5	302.9	0.813	0.036	0.816
303.6	302.9	0.970	0.042	0.975
503.2	302.9	1.224	0.054	1.235
503.5	302.9	1.227	0.054	1.238
702.8	302.9	1.396	0.066	1.414
752.5	302.9	1.438	0.069	1.458
902.2	302.9	1.519	0.078	1.544
902.6	302.8	1.532	0.078	1.558
902.8	302.8	1.527	0.078	1.553
104.6	282.8	0.753	0.033	0.755
503.0	282.8	1.526	0.064	1.541
901.7	282.8	1.792	0.088	1.824
105.6	263.1	1.104	0.043	1.106
502.4	263.1	1.812	0.072	1.831
901.5	263.1	2.038	0.098	2.078
106.1	243.8	1.484	0.053	1.488
304.4	243.8	1.905	0.068	1.918
503.9	243.8	2.090	0.082	2.114
703.3	243.8	2.197	0.094	2.233
901.7	243.8	2.304	0.109	2.353
902.5	243.8	2.294	0.108	2.343

Table 2 Equilibrium excess (Q^*_{ex,N_2}) and absolute (Q^*_{abs,N_2}) adsorption capacities of N_2 on H^+-mordenite measured on the DCB apparatus at a feed flow rate of 68.1 μmol s^{-1} of pure N_2. The uncertainty $u\left(Q^*_{ex,N_2}\right)$ in the adsorption capacity measurement is also reported

Nitrogen				
P (kPa)	T (K)	Q^*_{ex,N_2} (mmol g^{-1})	$u\left(Q^*_{ex,N_2}\right)$ (mmol g^{-1})	Q^*_{abs,N_2} (mmol g^{-1})
107.3	302.8	0.166	0.013	0.166
107.5	302.9	0.165	0.015	0.165
107.6	302.9	0.166	0.013	0.166
107.6	302.8	0.167	0.013	0.167
109.5	302.8	0.168	0.015	0.168
153.2	302.9	0.227	0.016	0.228
207.9	302.9	0.295	0.020	0.296
303.9	302.9	0.397	0.025	0.399
503.0	302.9	0.582	0.038	0.587
503.4	302.9	0.582	0.037	0.587
504.0	302.9	0.587	0.039	0.592
702.9	302.9	0.729	0.049	0.737
752.6	302.9	0.761	0.053	0.770
902.7	302.8	0.868	0.062	0.881
902.8	302.9	0.856	0.061	0.868
903.0	302.9	0.904	0.065	0.917
107.3	282.8	0.265	0.019	0.265
503.7	282.8	0.824	0.045	0.831
902.3	282.8	1.127	0.072	1.145
108.3	263.1	0.448	0.027	0.449
503.3	263.1	1.137	0.056	1.148
901.4	263.1	1.437	0.083	1.461
108.4	243.7	0.739	0.037	0.741
304.3	243.8	1.235	0.053	1.242
503.8	243.8	1.484	0.067	1.499
703.2	243.8	1.648	0.082	1.671
901.3	243.7	1.760	0.096	1.792
902.7	243.8	1.802	0.096	1.835

Table 3 Best fit parameters and their statistical uncertainties for the Langmuir model (Eq. (1)) together with the root mean square deviation (r.m.s.d.) of the model from the data, which also included the data of Jensen et al. (2012) and Hofman et al. (2012)

	$Q_{m,i}$ (mmol g^{-1})	10^7 $b_{0,i}$ (kPa^{-1})	$-\Delta H_i$ (kJ mol^{-1})	r.m.s.d. (mmol g^{-1})
CH_4	2.341 ± 0.021	5.85 ± 1.31	20.87 ± 0.58	0.036
N_2	2.262 ± 0.020	4.32 ± 0.33	18.58 ± 0.20	0.011

least-squares regression analysis to determine the best-fit parameters of the temperature-dependent Langmuir model:

$$Q^*_{abs,i} = \frac{Q_{m,i} b_i p_i}{1 + \sum_j^n b_j p_j} \text{ with } b_i = b_{0,i} \exp\left(\frac{-\Delta H_i}{RT}\right), \quad (1)$$

where $Q^*_{abs,i}$ is the absolute equilibrium adsorption capacity of adsorbate 'i', p_i is the partial pressure of the adsorbate, T is the gas temperature, R is the molar gas constant and ΔH_i is the isosteric enthalpy of adsorption at zero coverage. In the regression, ΔH_i was treated as an adjustable parameter along with the two empirical parameters $Q_{m,i}$ and $b_{0,i}$. Equation (1) represents the Extended Langmuir isotherm which reduces to the Langmuir isotherm when the number of components (n) is set to one. The least-squares regressions were conducted with $n = 1$ to the pure adsorbate data and the best-fit parameters, along with their associated statistical uncertainties, are listed in Table 3. Also shown in Table 3 is the root mean square (r.m.s.) deviation of the model from the measured data for each component. In both cases, the r.m.s. deviations were smaller than the average of the uncertainties in $Q^*_{ex,i}$ listed in Tables 1 and 2.

Delgado et al. (2006a) reported Toth isotherm parameters for H^+-mordenite obtained by regression of experimental data measured at temperatures ranging from 279 to 308 K and at pressures up to 2,000 kPa. As found by Hofman et al. (2012) the model of Delgado et al. was consistent with the capacities measured here at 302.9 K. However, when the model of Delgado et al. was extrapolated to 243.9 K the deviations between the measured and predicted capacities increased up to 0.25 mmol g^{-1}, which was about 10 % of the measured capacity and twice the experimental uncertainty.

The total and component adsorption capacities for CH_4 and N_2 on H^+-mordenite measured at temperatures in the range 243.8–302.9 K in the DCB for approximately equimolar $CH_4 + N_2$ mixtures are listed in Table 4 and shown as a function of mixture pressure in Fig. 2. Also shown are calculated adsorption capacities for each component predicted from the pure fluid Langmuir isotherms (Eq. (1), Table 3) using the Ideal Adsorbed Solution Theory (IAST) developed by Myers and Prausnitz (1965) and implemented

Table 4 Excess ($Q^*_{ex,i}$) and absolute ($Q^*_{abs,i}$) adsorption capacities determined from the DCB measurements with $CH_4 + N_2$ mixtures. Also listed are the adsorption selectivities $(\alpha_{CH_4:N_2})_{meas}$ of CH_4 over N_2 on H^+-mordenite. The average uncertainty in $(\alpha_{CH_4:N_2})_{meas}$ is ±0.4

P (kPa)	T (K)	y_{CH_4} (–)	Q^*_{ex,CH_4} (mmol g^{-1})	$u(Q^*_{ex,CH_4})$ (mmol g^{-1})	Q^*_{abs,CH_4} (mmol g^{-1})	Q^*_{ex,N_2} (mmol g^{-1})	$u(Q^*_{ex,N_2})$ (mmol g^{-1})	Q^*_{abs,N_2} (mmol g^{-1})	$(\alpha_{CH_4:N_2})_{meas}$ (–)
106.0	302.9	0.49	0.274	0.020	0.275	0.076	0.018	0.076	3.7
108.2	302.8	0.50	0.282	0.019	0.283	0.076	0.018	0.076	3.7
304.0	302.9	0.49	0.592	0.038	0.596	0.161	0.032	0.162	3.8
503.1	302.9	0.49	0.785	0.052	0.793	0.215	0.043	0.217	3.8
703.0	302.9	0.48	0.898	0.065	0.911	0.267	0.053	0.271	3.6
902.2	302.9	0.48	1.005	0.076	1.024	0.295	0.063	0.301	3.7
902.4	302.9	0.47	0.980	0.076	0.999	0.294	0.062	0.300	3.8
902.9	302.8	0.49	1.014	0.076	1.033	0.285	0.062	0.290	3.7
105.8	282.9	0.50	0.451	0.027	0.452	0.111	0.024	0.111	4.1
502.7	282.9	0.50	1.054	0.064	1.066	0.259	0.047	0.262	4.1
901.7	282.9	0.49	1.221	0.086	1.246	0.335	0.067	0.342	3.8
107.4	263.2	0.50	0.730	0.038	0.732	0.155	0.031	0.155	4.7
503.3	263.1	0.49	1.313	0.076	1.329	0.313	0.052	0.317	4.4
902.0	263.1	0.49	1.501	0.101	1.535	0.370	0.075	0.378	4.2
107.8	243.8	0.50	1.073	0.052	1.076	0.205	0.034	0.206	5.2
303.4	243.9	0.50	1.448	0.074	1.460	0.284	0.040	0.286	5.1
503.2	243.8	0.50	1.600	0.088	1.622	0.332	0.053	0.336	4.8
702.5	243.9	0.49	1.699	0.102	1.731	0.360	0.066	0.367	4.9
901.7	243.9	0.49	1.769	0.116	1.813	0.386	0.081	0.396	4.8
902.4	243.8	0.49	1.758	0.115	1.801	0.386	0.080	0.396	4.7

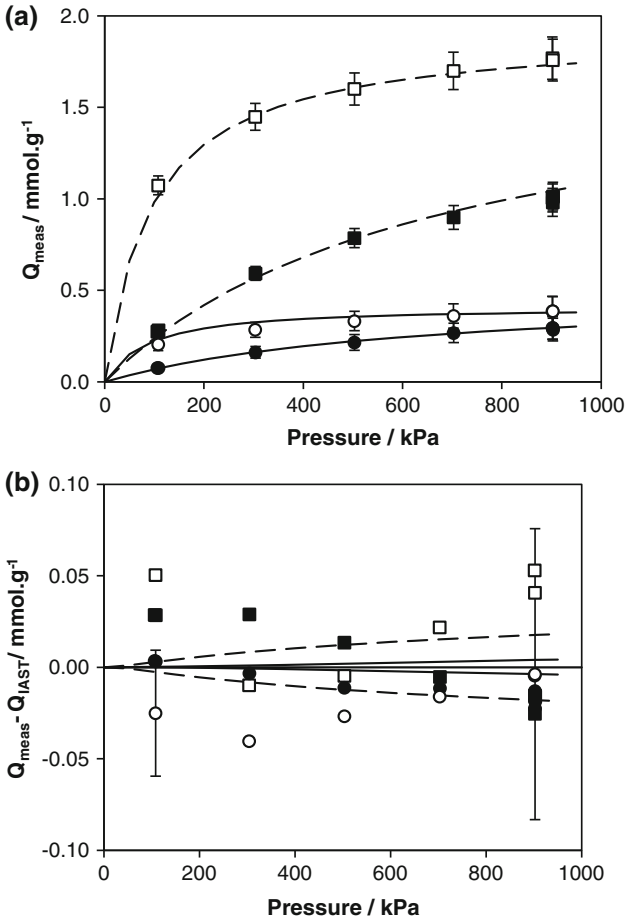

Fig. 2 Measured and modeled adsorption capacities for each component in an equimolar CH_4 and N_2 gas mixture as a function of the mixture's total pressure. **a** Absolute adsorption capacity for CH_4 (*squares*) and N_2 (*circles*) at 302.9 K (*solid symbols*) and 243.8 K (*open symbols*). *Curves* represent the IAST-Langmuir predicted capacities. **b** Deviation of the measured capacities (*points*) and Extended Langmuir isotherm (*curves*) (Eq. (1)) from the IAST prediction. The *error bars* show the representative uncertainty of the measurements at 100 and 900 kPa

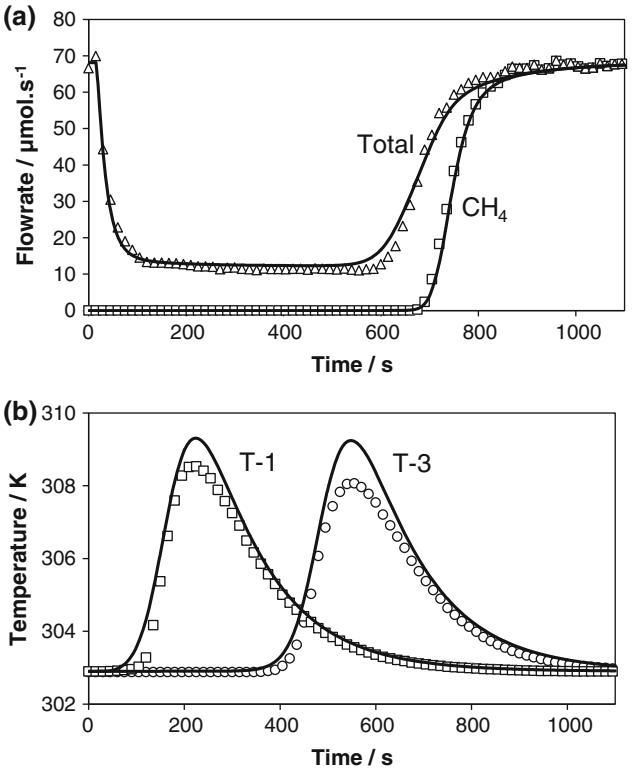

Fig. 3 Breakthrough of CH_4 at 503.2 kPa, 302.9 K showing both the data (*points*) and the model predictions (*curves*). **a** Adsorbate and total flow rate at the column outlet. The difference between two flow rates is due to the He that was initially in the bed (for clarity the helium effluent flow is not shown). **b** Temperature time series recorded by thermometers 1 and 3. Experimental data were collected at 1 s intervals with not all points shown here

using the algorithm of Valenzuela and Myers (1989). No parameters were adjusted within the IAST models, and as shown in Fig. 2b, the agreement between the IAST predictions and the measured mixture capacities was excellent.

Although the IAST provided accurate predictions of the equilibrium component adsorption capacities, the iterative calculations required in the implementation of the IAST add significantly to the computational time required when using a full dynamic model of the DCB experiments for the prediction of breakthrough curves. Thus, in the dynamic model of the DCB experiments, we used the Extended Langmuir isotherm (Eq. (1) with $n = 2$) with the pure fluid parameters listed in Table 3 to predict the equilibrium component adsorption capacities for mixtures.

A comparison of the Extended Langmuir and IAST predictions is shown in Fig. 2b and the discrepancy between the models was small. The maximum deviation between the IAST-Langmuir and Extended Langmuir predictions was 0.02 mmol g^{-1}, which is within the uncertainty of the measured mixture capacities.

3 Analysis of dynamic data

Figure 3 shows a characteristic set of dynamic effluent flow rate and temperature data measured during an experiment with pure CH_4. The bed initially contained helium and this is the reason for the difference between the adsorbate (CH_4 in Fig. 3) and the total flow rates. (The effluent helium flow rate was measured but is not shown in Fig. 3 for clarity.) To extract information about the adsorption kinetics from this data, a dynamic model was constructed with a minimal number of adjustable parameters for the purpose of data regression. Similar models have been reported by several researchers including Ackley and Yang (1990), Simo et al. (2008) and Warmuzinski and Tanczyk (1997). Although

the fundamental mass and energy balances used in each of these models have many similarities, each DCB model must account for the effects of the particular experimental configuration employed. The model of our DCB apparatus experiments was based on the following set of assumptions:

1. The gas phase was ideal.
2. There were no mass, heat and momentum gradients in the radial direction.
3. The bed hydrodynamics were described by plug flow with axial mass dispersion.
4. The mass transfer rate between the gas and adsorbed phases was described using the LDF approximation with a lumped MTC.
5. The adsorption of helium was neglected under the conditions studied.
6. The momentum balance was described using the Ergun equation.

A schematic of the model used to represent the experimental system is shown in Fig. 1b. In addition to the packed adsorbent bed, the system includes other components that together contained approximately the same volume of gas as there was in the void spaces of the packed bed. The volume of these extra components must be included in the dynamic model of DCB apparatus to account for the additional retention time and band broadening present in experimental breakthrough curves (Rajendran et al. 2008). The volumes of each of the extra-column void spaces are shown in Fig. 1b and were measured using three independent methods as described by Hofman et al. (2012), amounting in total to 36 ± 2 cm^3. The inlet and outlet tubes were modeled as ideal plug flow reactors (PFRs) and the inlet and outlet cones connecting the column to inlet and outlet tubes were modeled as ideal continuous stirred tank reactors (CSTRs). A performance test of these models for the extra-column void spaces is presented in Sect. 4.

The packed column was modeled by solving numerically the differential equations presented below describing its material and energy balances. The model's initial and boundary conditions were chosen so as to match the system variables that were controlled or monitored experimentally. The initial gas phase composition was set to be pure helium throughout the apparatus and the adsorbed amounts of all species throughout the bed were set to be zero. The column's inlet boundary condition was set to be a constant flow rate (corresponding to that defined by the MFCs) while its outlet boundary had a constant pressure specification, as set by the BPR. The initial condition of the adsorbate concentration front was taken to be a step function located at the inlet tube's upstream boundary. This step function was smeared out by the CSTR model prior to the column, which assisted with the stability of the numerical solutions determined by the model. As discussed below, the gas composition and velocity calculated using the numerical model were compared with the effluent component flow rates measured with the MFM and MS, either to determine MTCs by regression and/or to test breakthrough predictions for binary adsorbate mixtures. Values for the parameters in the model that were held constant for the H^+-mordenite experiments are listed in Table 5.

The differential equations solved numerically to describe the column included the material balance for each component i as shown in Eq. (2). This included terms for (from left to right): dispersion and convection in the inter-particle gas phase, accumulation in the inter-particle gas phase, accumulation in the intra-particle gas phase, and accumulation in the adsorbed phase.

$$-\varepsilon_b \frac{\partial}{\partial z}\left(D_{ax,i}\frac{\partial c_{b,i}}{\partial z}\right) + \varepsilon_b \frac{\partial\left(v_g c_{b,i}\right)}{\partial z} + \varepsilon_b \frac{\partial c_{b,i}}{\partial t} + (1-\varepsilon_b)\varepsilon_p \frac{\partial c_{p,i}}{\partial t} + \rho_s \frac{\partial Q_i}{\partial t} = 0, \quad (2)$$

where $D_{ax,i}$ is the axial dispersion coefficient for component i; $c_{b,i}$ and $c_{p,i}$ are the molar concentrations (in moles per unit volume) of species i in the inter-particle and intra-particle gas phase, respectively; v_g is the interstitial gas velocity; ρ_s is the bulk solid density; ε_b and ε_p are the bed

Table 5 Values of the constants used in the dynamic model of the DCB experiments conducted with H^+-mordenite

Parameter	Value
Bed height, H_{bed}	130 mm
Bed diameter, D_{bed}	22.2 mm
Bed wall thickness, W_T	1.55 mm
Inter-particle voidage, ε_b	0.559
Intra-particle voidage, ε_p	0.463
Bulk density, ρ_s	601 kg m^{-3}
Pellet radius, r_p	0.91 mm
Pellet shape factor, Φ	0.734
Adsorbed phase heat capacity (He), $C_{pa,i}$	20 J mol^{-1} K^{-1}
Adsorbed phase heat capacity (CH_4), $C_{pa,i}$	35 J mol^{-1} K^{-1}
Adsorbed phase heat capacity (N_2), $C_{pa,i}$	29 J mol^{-1} K^{-1}
Adsorbent thermal conductivity, λ_s	0.5 W m^{-1} K^{-1}
Wall thermal conductivity, λ_w	16 W m^{-1} K^{-1}
Adsorbent heat capacity, $C_{p,s}$	1.0–1.5 J g^{-1} K^{-1}
Wall specific heat, $C_{p,w}$	0.5 J g^{-1} K^{-1}
Wall-ambient heat transfer coefficient, h_{wa}	3,000 W m^{-2} K^{-1}
Specific surface area of adsorbent, a_p	1,458 m^{-1}

and particle void fractions, respectively; z is the column's axial position coordinate; and t is time.

The axial dispersion coefficient was estimated using the method described by Delgado (2006), which assumes that the diffusive and convective components of dispersion are additive:

$$\frac{D_{ax,i}}{D_{m,i}} = \frac{1}{\Gamma_b} + \frac{Pe_{p,i}}{2} \text{ with } Pe_{p,i} = \frac{v_g d_p}{\varepsilon_b D_{m,i}}, \quad (3)$$

where $D_{m,i}$ is the molecular diffusivity of species i into He, $Pe_{p,i}$ is the particle Péclet number and d_p is the particle diameter. The tortuosity Γ_b was calculated from the relation proposed by Lanfrey et al. (2010)

$$\Gamma_b = 1.23\frac{(1-\varepsilon_b)^{4/3}}{\varepsilon_b \phi^2} \text{ with } \phi = \frac{\left(36\pi V_p^2\right)^{1/3}}{S_p} \quad (4)$$

where the particle shape factor or sphericity ϕ is defined from the volume V_p and surface area S_p of a single particle. The H^+-mordenite pellets used in this investigation were cylindrical with a sphericity of 0.734.

The molecular diffusivity for each component was calculated using the Chapman–Enskog theory of gaseous diffusion as described by Reid et al. (1987). In the multi component experiments, the molecular diffusivity of the mixture's component i into helium was estimated using (Bird et al. 2002)

$$D_{m,i} = \frac{1-y_i}{\sum_{\substack{j=1 \\ j\neq i}}^{n} \frac{y_j}{D_{i,j}}} \quad (5)$$

The rate of mass transfer for each component from the gas to the adsorbed phase was modeled using the LDF approximation with a lumped MTC_i (Yang 1997) (Sircar and Hufton 2000)

$$\frac{\partial Q_i}{\partial t} = MTC_i\left(Q^*_{abs,i} - Q_i\right) \quad (6)$$

The equilibrium capacity $Q^*_{abs,i}$ is generally evaluated based on the intra-particle gas phase concentration $c_{p,i}$. In this work, we assumed that $c_{p,i}$ was equal to the inter-particle gas phase concentration $c_{b,i}$, which is proportional to the partial pressure of the component; that is, the $Q^*_{abs,i}$ were evaluated using Eq. (1) from the partial pressure of each component in the column's bulk gas phase. This assumption was made because: (i) it simplified the implementation of the model, (ii) no independent information about the $c_{p,i}$ were available from the DCB experiment and (iii) because the $Q^*_{abs,i}$ used in the evaluation of the MTC_i were obtained from measurements with this DCB apparatus. The effect of this assumption is to combine in series all the resistances to mass transfer (film, macropore, micropore) between the bulk inter-particle gas phase and the adsorbed phase. Consequently, the lumped mass transfer coefficient MTC_i used in Eq. (6) (which is inversely proportional to mass transfer resistance) characterizes the cumulative effect of these various mass transfer barriers. As a result, in many cases the numerical value of the MTC_i will be largely set by the mass transfer mechanism with the greatest resistance.

The determination of MTC_i via a least-squares regression to the dynamic data was the principal objective of the modeling. To achieve this objective reliably it was also necessary, in general, to describe and solve the energy balances for the adsorbent bed, the inter-particle gas phase, and the column wall.

The model of the packed adsorbent bed included the solid adsorbent particle phase, the adsorbed fluid phase and the intra-particle gas phase. The energy balance for the adsorbent bed is shown in Eq. (7) and included terms for (from left to right): thermal conduction in the solid, accumulation of heat in the intra-particle gas phase, accumulation of heat in the solid phase and in the adsorbed phase, the heat of adsorption, and heat transfer from the adsorbent particles to the inter-particle gas phase.

$$-\lambda_s(1-\varepsilon_b)\frac{\partial^2 T_s}{\partial z^2} + C_{p,s}\rho_s\frac{\partial T_s}{\partial t} + \rho_s\sum_i\left(C_{pa,i}Q_i\right)\frac{\partial T_s}{\partial t} + \rho_s\sum_i\left(\Delta H_i\frac{\partial Q_i}{\partial t}\right) + h_{sg}a_p\left(T_s - T_g\right) = 0, \quad (7)$$

where λ_s is the solid phase thermal conductivity, T_s and T_g are the solid and gas phase temperatures respectively, $C_{p,s}$ is the solid phase specific heat capacity, $C_{pa,i}$ is the adsorbed phase specific heat capacity, h_{sg} is the solid to gas phase heat transfer coefficient and a_p is the particle surface area per unit volume of the column.

The energy balance for the inter-particle gas phase is shown in Eq. (8) and included terms for (from left to right): thermal conduction and thermal convection, accumulation of heat, gas compression, heat transfer from gas to the solid adsorbent, and heat transfer from gas to the column's inner wall.

$$-\lambda_g\varepsilon_b\frac{\partial^2 T_g}{\partial z^2} + C_{v,g}\rho_g v_g\frac{\partial T_g}{\partial z} + C_{v,g}\rho_g\varepsilon_b\frac{\partial T_g}{\partial t} + p\frac{\partial v_g}{\partial z} + h_{sg}a_p\left(T_g - T_s\right) + h_{gw}\frac{4}{D_{bed}}\left(T_g - T_w\right) = 0 \quad (8)$$

where λ_g is the gas phase thermal conductivity, $C_{v,g}$ is the gas phase specific heat capacity at constant volume, ρ_g is the gas phase density, p is the pressure, h_{gw} is the gas phase to column wall heat transfer coefficient, D_{bed} is the column diameter and T_w is the column wall temperature.

The energy balance for the column wall included terms for (from left to right): axial thermal conduction along the wall, accumulation of heat in the wall, heat transfer from

the gas to the inner wall, and heat transfer from the outer wall to the environment at temperature T_a.

$$-\lambda_w \frac{\partial^2 T_w}{\partial z^2} + \rho_w C_{p,w} \frac{\partial T_w}{\partial t} + h_{gw} \frac{4d_c}{(D_{bed} + W_T)^2 - D_{bed}^2} (T_w - T_g) + h_{wa} \frac{4(D_{bed} + W_T)}{(D_{bed} + W_T)^2 - D_{bed}^2} (T_w - T_a) = 0, \quad (9)$$

where λ_w is the wall thermal conductivity, ρ_w is the wall density, $C_{p,w}$ is the wall specific heat capacity, W_T is the wall thickness, h_{wa} is the wall to ambient heat transfer coefficient and T_a is the ambient temperature.

Within the range of conditions over which the breakthrough apparatus operates, the heat transfer coefficient, h_{sg} was estimated using the following equation (Bird et al. 2002)

$$h_{sg} = 1.66 C_{p,g} v_g \rho_g \, \mathrm{Pr}^{-2/3} \, \mathrm{Re}^{-0.51} \quad (10)$$

with

$$\mathrm{Pr} = \frac{\mu C_{p,g}}{\lambda_g M} \text{ and } \mathrm{Re} = \frac{2 r_p M \rho_g v_g}{\mu},$$

where μ is the gas viscosity, M is the gas molecular weight and r_p is the particle radius. The heat transfer coefficient between the gas phase and column wall, h_{gw}, was estimated using a correlation based on the work of Kast (1988):

$$Nu_w \left(1 + \frac{12 H_{bed}}{D_{bed} Pe_H}\right) = -2 \times 10^{-6} (Pe_H)^2 + 0.0477 Pe_H + 22.11 \quad (11)$$

with

$$Nu_w = \frac{h_{gw} x_{char}}{\lambda_g} \text{ and } Pe_H = \frac{x_{char} v_g \rho_g M C_{p,g}}{\lambda_g},$$

where H_{bed} is the column length and the characteristic length is defined as $x_{char} = 1.15(2r_p)$.

The dynamic model was implemented in, and solved using, Aspen Adsorption V7.1 (Aspen Technology, Inc., Massachusetts); a commercial adsorption software package that uses the method of lines (Schiesser 1991) to solve the time-dependent partial differential equations. Importantly, the results of this Aspen Adsorption implementation of the model were checked against a simplified, isothermal, model implemented in the software LabVIEW V9.0 (National instruments, Texas). The agreement between the two models was reasonable in cases where the observed experimental temperature increases due to adsorption were less than about 6 K. This magnitude increase in bed temperature was generally observed for experiments with H^+-mordenite conducted at 303 K. In such cases, the values of the *MTC* parameter determined using the isothermal model were about half of the values derived with the full energy balance and reported here. At lower temperatures, for which adsorption capacities are larger, bed temperatures during an experiment increased by up to 10 K and, under these conditions, the agreement between the isothermal and full energy balance models became significantly worse. As a further check, the Aspen Adsorption model was modified to operate isothermally and, in this configuration, the agreement with the MTC_i extracted using the LabVIEW-based model was within 10 %, which was within the statistical uncertainty of the regression. The implementation of Eq. (7) in Aspen Adsorption does not include the factor of $(1 - \varepsilon_b)$ in the axial conduction term of the solid phase energy balance. This could be corrected by reducing the effective value of λ_s. However, the impact of such a correction is insignificant because the conduction term is about three orders of magnitude smaller than the heat transfer from the solid to the gas phase.

4 Estimation of adsorption kinetic parameters for pure fluids

To ensure that the extra-column void volumes were correctly modeled, preliminary breakthrough measurements were conducted with the column removed from the DCB apparatus and the inlet and outlet conical sections connected together directly (see Fig. 1). Breakthrough experiments with N_2 were conducted at 302 K and pressures of 109 and 793 kPa, and the results are shown in Fig. 4. The data were compared with the predictions of the combined PFR and CSTR models of the tubes and cones that comprised the extra-column volumes, and the agreement was found to be excellent at both pressures.

To minimize the significant effects of parameter correlation on the predicted effluent flows, the MTC was the only quantity adjusted in the dynamic model during data regression. The values for several other parameters needed in the model were estimated using available literature data and the sensitivity of these parameters were investigated to determine what, if any, effect they had on the results.

The first parameters studied were the three heat transfer coefficients. Using Eqs. (10) and (11), the values of h_{sg} and h_{gw} for our DCB experiment were calculated to be in the range 25–100 and 25–60 W m^{-2} K^{-1} respectively. The heat transfer coefficient from the column wall to the environment, h_{wa}, was more difficult to estimate: Bird et al. (2002) estimated that heat transfer coefficients in such systems range between 500 and 10,000 W m^{-2} K^{-1}. The method of Churchill and Bernstein (1977) suggests an h_{wa}

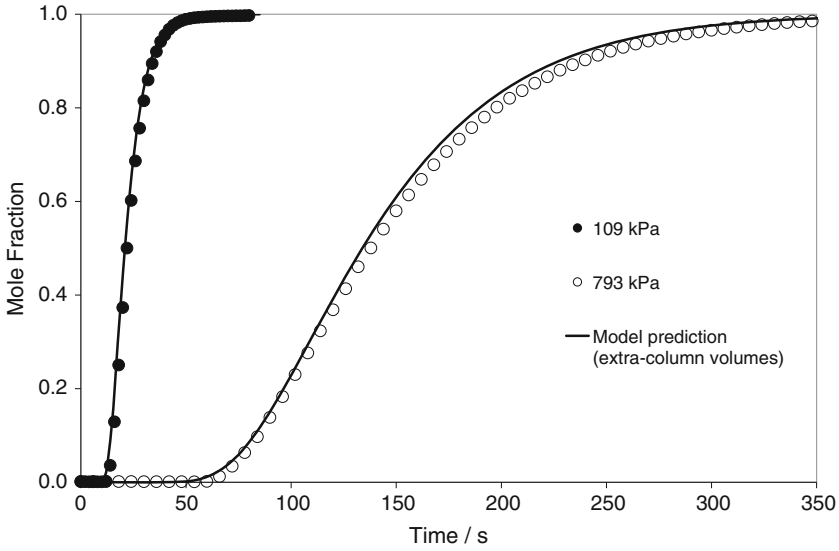

Fig. 4 Breakthrough of N_2 at 302.9 K measured with the column removed from the DCB apparatus and the two cones connected directly together. These data (*points*) were collected to test the model (*curves*) of the extra-column void volumes. Experimental data were collected at 1 s intervals with not all points shown here

around 1,000 W m^{-2} K^{-1}; however their correlation is valid for cylinders subject only to a constant cross flow, whereas the circulating bath used in this study had both a significant flow in the axial direction as well as cross flow that varied along the length of the column. To determine the sensitivity of our results to h_{wa} we tested values over the range 10^{-2}–10^{6} W m^{-2} K^{-1}. Below 300 W m^{-2} K^{-1}, the effect of h_{wa} on the overall heat transfer coefficient (the series combination of h_{sg}, h_{gw} and h_{wa}) became greater than 5 % causing the temperature profiles to take significantly longer to return to the ambient temperature. For $h_{wa} > 300$ W m^{-2} K^{-1}, the impact on the calculated bed temperature profiles was small, and the calculated temperature profile was insensitive to variation in values of h_{wa} above 1,000 W m^{-2} K^{-1}. The value of h_{wa} was thus set to 3,000 W m^{-2} K^{-1} for all subsequent data analysis, with a typical temperature profile shown in Fig. 3.

The second parameter studied was the specific heat capacity of the adsorbent, $C_{p,s}$. This value was estimated to be 1.5 J g^{-1} K^{-1} at a temperature of 303 K (Mohamed 2001) which resulted in a good agreement between the observed and calculated temperature profiles as shown, for example, in Fig. 3b. While the heat capacity did have a large influence on the magnitude of the calculated temperature increase in the column, it did not significantly affect the material balance calculations and, hence, the results of the MTC extraction. For example, if a heat capacity of 1.0 J g^{-1} K^{-1} (−33 %) was used, the extracted MTC_i decreased by only 1.9 %.

At 243 K, it was necessary to increase $C_{p.s}$ by 50 % to achieve the same level of agreement between the measured and calculated peak-bed temperatures achieved at 303 K. The key differences between our experiments and those in which Mohamed (2001) measured mordenite's $C_{p.s}$ were that we used pellets of mordenite, which also contained a binding material. In contrast Mohamed reported the $C_{p.s}$ mordenite crystals and did not report heat capacity measurements for mordenite below 303 K. The effective heat capacity of the sample is sensitive to both these material and temperature effects. However, the MTCs extracted from the DCB experimental data were found to be insensitive to the precise value of $C_{p.s}$ used.

To maximize the fit quality for a given set of dynamic data (i.e. at fixed *T, p*) and to ensure that the dynamic material balance was self-consistent once equilibrium was achieved, it was necessary to slightly adjust the value of $Q_{m.i}$ in Eq. (1) from the value listed in Table 3. The equilibrium capacities calculated using the Langmuir model deviated from those obtained directly from the dynamic data (using the method described by Hofman et al. (2012) by an amount comparable with the capacities' experimental uncertainty because the Langmuir model was regressed to multiple measurements made over a wide range of conditions. Thus, while the Langmuir models for CH_4 and N_2 represent the best global descriptions of the equilibrium adsorption capacities, their uncorrected use in the regression of the dynamic model to data measured at a single temperature and pressure resulted in poorer fits and less reliable values of the MTC_i. The required adjustment of $Q_{m,i}$ was on average ± 3 %, which is consistent with the relative r.m.s. deviations of the Langmuir models from the data to which they were regressed (3 % for CH_4, 2 % for N_2). The sensitivity of the regression to the value of $Q_{m.i}$ used was tested by performing the same extraction with and without the adjustment of $Q_{m.i}$. The case chosen was the pure CH_4 experiment at temperature and pressure conditions of 302.9 K and 104.9 kPa, which had the largest discrepancy between the measured and Langmuir-predicted

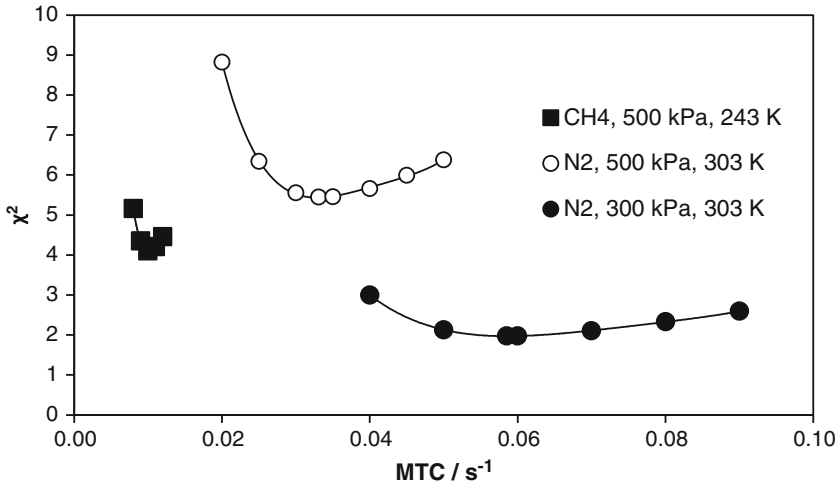

Fig. 5 Examples of the manual determination of the objective function's minimum. The *plot* shows CH_4 and N_2 extractions with MTC_i values of 0.010, 0.033 and 0.059 s^{-1}, χ^2 values of 4.1, 5.4 and 2.0 (Eq. (13)) and relative MTC_i uncertainties of −20.3, +36.0, −24.2, +55.7 and −31.9, +74.0 %, respectively

Table 6 MTC_i for CH_4 and N_2 extracted from pure fluid DCB measurements at a feed flowrate of 68.1 μmol s^{-1}. The lower and upper bounds of the 68 % confidence intervals for the MTC_i are given together with the r.m.s.d. of the measured flows from those calculated with the regressed dynamic models

	T (K)	P (kPa)	MTC_i (s^{-1})	Lower (s^{-1})	Upper (s^{-1})	r.m.s.d. (μmol s^{-1})
CH_4	302.9	153.0	0.044	0.035	0.061	2.0
	302.9	207.5	0.042	0.031	0.060	2.2
	302.9	303.6	0.029	0.022	0.042	1.7
	302.9	503.2	0.021	0.016	0.030	1.3
	302.9	702.8	0.013	0.010	0.018	1.7
	302.9	902.2	0.013	0.010	0.017	3.9
	282.8	503.0	0.016	0.013	0.023	1.7
	282.8	901.7	0.0063	0.0054	0.0077	2.5
	263.0	502.4	0.014	0.010	0.018	1.8
	263.0	901.5	0.0050	0.0043	0.0058	2.8
	243.6	304.4	0.018	0.013	0.027	2.5
	243.6	503.9	0.010	0.008	0.014	1.8
	243.6	703.3	0.0065	0.0055	0.0078	2.0
	243.6	901.7	0.0040	0.0036	0.0046	3.0
N_2	302.9	153.2	0.10	0.08	0.16	2.7
	302.9	207.9	0.085	0.062	0.129	2.8
	302.9	303.9	0.059	0.040	0.103	1.3
	302.9	503.4	0.033	0.025	0.051	2.1
	302.9	702.9	0.017	0.014	0.024	2.1
	302.9	902.8	0.011	0.009	0.014	3.1
	282.8	503.7	0.027	0.020	0.039	1.9
	282.8	902.3	0.0086	0.0074	0.0104	3.7
	263.0	503.3	0.017	0.013	0.023	1.6
	263.0	901.4	0.0065	0.0055	0.0077	3.8
	243.6	304.3	0.025	0.019	0.039	1.9
	243.5	503.8	0.013	0.010	0.018	1.8
	243.6	703.2	0.0074	0.0062	0.0090	2.8
	243.5	901.3	0.0050	0.0043	0.0059	4.1

capacity, of 6.6 %. Using the Langmuir predicted capacity decreased the fit quality by a factor of 4.5 (i.e. increased the objective function defined by Eq. (13) by this amount) and increased the value of MTC_i obtained from the regression by 58 %.

The MTC_i values for both pure fluids at a given temperature and pressure were estimated by regression of the model to the dynamic data in the following manner. With all other model parameters estimated and fixed, an initial value of MTC_i was selected (usually with guidance from previous results) and the model was solved numerically. Component molar flow rates at each point in time were calculated at the location of the MFM (after Outlet Tube 2 in Fig. 1b) using

$$F_{i,\mathrm{calc}} = c_{b,i} v_g A_{tube} \tag{12}$$

where A_{tube} is the area of the outlet tube. The value of the objective function, χ^2, for the assumed MTC_i was then evaluated using

$$\chi^2 = \frac{1}{Np - x - 1} \sum_{i=1}^{N} \sum_{j=1}^{p} \frac{\left(F_{i,\mathrm{meas}}(t_j) - F_{i,\mathrm{calc}}(t_j)\right)^2}{\left\langle u\left(F_{i,\mathrm{meas}}\right)\right\rangle}, \tag{13}$$

where $F_{i,meas}(t_j)$ and $F_{i,calc}(t_j)$ are, respectively, the measured and calculated effluent molar flow rate of each of the components (i) at time t_j, and $u(F_{i,meas})$ is the uncertainty of the flow rate measurement. The equation is summed over all time points (p) and gas species (N) before being normalized by the number of degrees of freedom where x is the number of fitted parameters (i.e. one, MTC_i). The angled brackets in Eq. (13) denote the average value over the duration of the experiment: the uncertainty in the effluent flow measurement used in evaluation of χ^2 was usually 0.82 μmol s^{-1} (1.2 sccm) (Hofman et al. 2012).

The search for the MTC_i value that minimized the objective function χ^2 was conducted manually. As shown by the examples in Fig. 5, the value of χ^2 was evaluated for a range of MTC_i values spanning the minimum. The examples shown in Fig. 5 highlight the ranges in value, shallowness and asymmetry of the minima obtained. In Table 6, the values of the MTC_i that minimized χ^2 at each temperature and pressure are presented, together with the corresponding r.m.s. deviation in the calculated flow rates to give an indication of the quality of the fit. Also listed are the lower and upper bounds of the 68 % confidence range in MTC_i. These bounds, which in general are not symmetric, correspond to the values of MTC_i at which χ^2 increased by 1 over the minimum value achieved (Bevington and Robinson 1992). It is clear from this analysis that the information content of the dynamic DCB data about the MTC_i parameters varied significantly over the range of conditions studied. Nevertheless, the primary purpose of estimating bulk MTC_i parameters is to enable

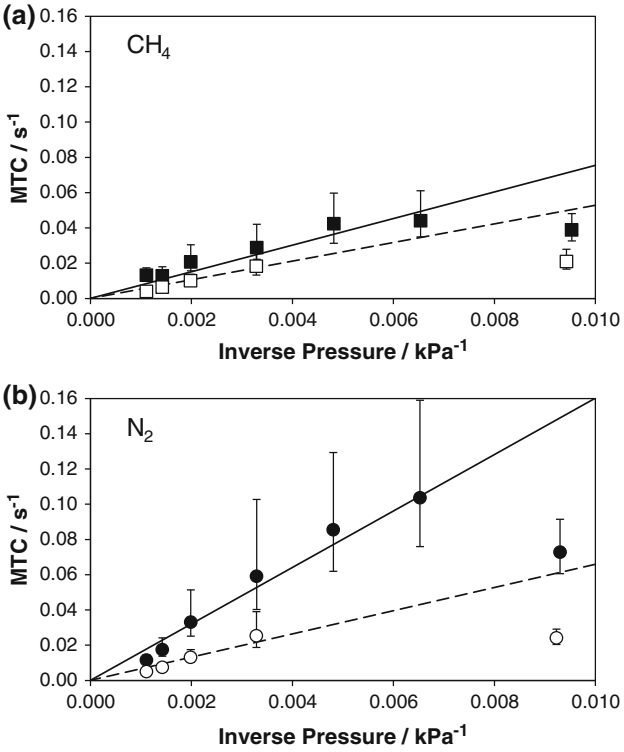

Fig. 6 Pressure and temperature dependence *of* MTC_i for **a** CH_4 (*squares*) and **b** N_2 (*circles*) at temperatures of 302.9 K (*closed symbols*) and 243.5 K (*open symbols*). The *lines* represent the best linear fit with a constrained intercept of zero. The *values* around 105 kPa ($\sim$0.095 kPa^{-1}) appear to be outliers and were excluded from the fit

predictions of mixture separation performance, and these quantitative estimates and analyses provide the necessary basis for assessing such predictions.

Figure 6 shows the extracted pure fluid MTC_i values plotted as a function of inverse pressure at different temperatures. The MTC_i values extracted for experiments at pressures lower than 110 kPa at all temperatures and for both gases were outliers relative to the linear trends exhibited by the higher pressure data. These anomalous values for the MTC_i are attributable to the turbo pump in the mass spectrometer: at low concentrations, the residence time of helium in the mass spectrometer (referred to as 'clean-up time' by the MS manual) was significantly longer than any other gas. As a result of this helium tail effect, the apparent breakthrough curves for pure adsorbates into helium at pressures less than 110 kPa were artificially smeared out, and consequently, the MTC_i values extracted from such breakthrough curves were biased to lower values.

Figure 7 shows a demonstration of this helium tail effect using four breakthrough experiments performed using the bypass loop (instead of the column) at 103 kPa. Bypassing the column produces the narrowest breakthrough profiles

achievable with the DCB apparatus and, therefore, maximizes the contrast achievable when helium tail effect is present with when it is not. It should be noted that this helium tail effect is a systematic error associated with the hold-up of helium in the mass spectrometer, and is not related to the column or the adsorbent. In the first experiment shown in Fig. 7, the system was initially filled with N_2 and a He breakthrough experiment was conducted (open symbols). The second experiment was a repeat of the first but with a CH_4 breakthrough into a system filled with N_2 (closed symbols). The results of these two experiments, shown in Fig. 7a, overlap each other and are as would be expected for such experiments. The third and fourth experiments were the opposite of the first two, with N_2 breaking through the column rather than being displaced. The results, displayed in Fig. 7b, show that when N_2 displaces CH_4 (solid symbols) the breakthrough curve matches those observed for the first and second experiment. However, for the N_2 breakthrough into He (open symbols) there is a significant deviation from other breakthrough profiles, with the profile being smeared out over an extended length of time producing a 'helium tail'. We found that this effect became less significant as the duration of the breakthrough increased, presumably beyond some characteristic pump-down time for helium. Only experiments conducted at pressures around 110 kPa or lower in this work had sufficiently short breakthrough durations for this helium tail to significantly affect the apparent effluent composition.

Furthermore, while the helium tail reduced the apparent MTC_i extracted at pressures below 110 kPa, its effect on the equilibrium adsorption capacities derived from the DCB data was negligible. As demonstrated by Hofman et al. (2012), capacities for single-adsorbate systems can be determined directly from the MFC and MFM readings without reference to the MS effluent composition measurement. When effluent composition measurements are needed to determine component capacities for two or more adsorbates, the helium tail's impact is mitigated by (i) its short duration in comparison with the time scale of the

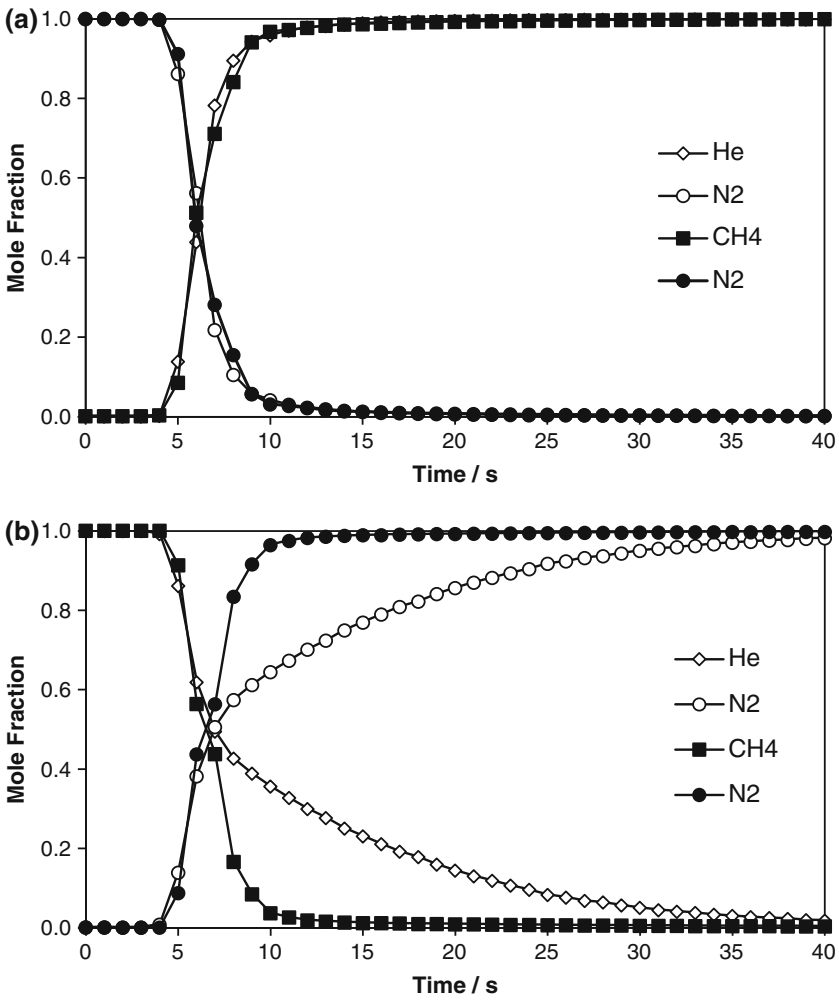

Fig. 7 Breakthrough profiles showing the effect of the 'helium tail' with effluent mole fraction compositions for N_2 (*circles*), He (*diamonds*) and CH_4 (*squares*) measured by the MS. **a** Breakthrough of He (*open*) and CH_4 (*closed*) into the bypass loop shown in Fig. 1, which initially contained N_2. (MPV-2 was switched to exclude the column from the flow path.) **b** Breakthrough of N_2 into the bypass loop, which initially contained He (*open*) or CH_4 (*closed*)

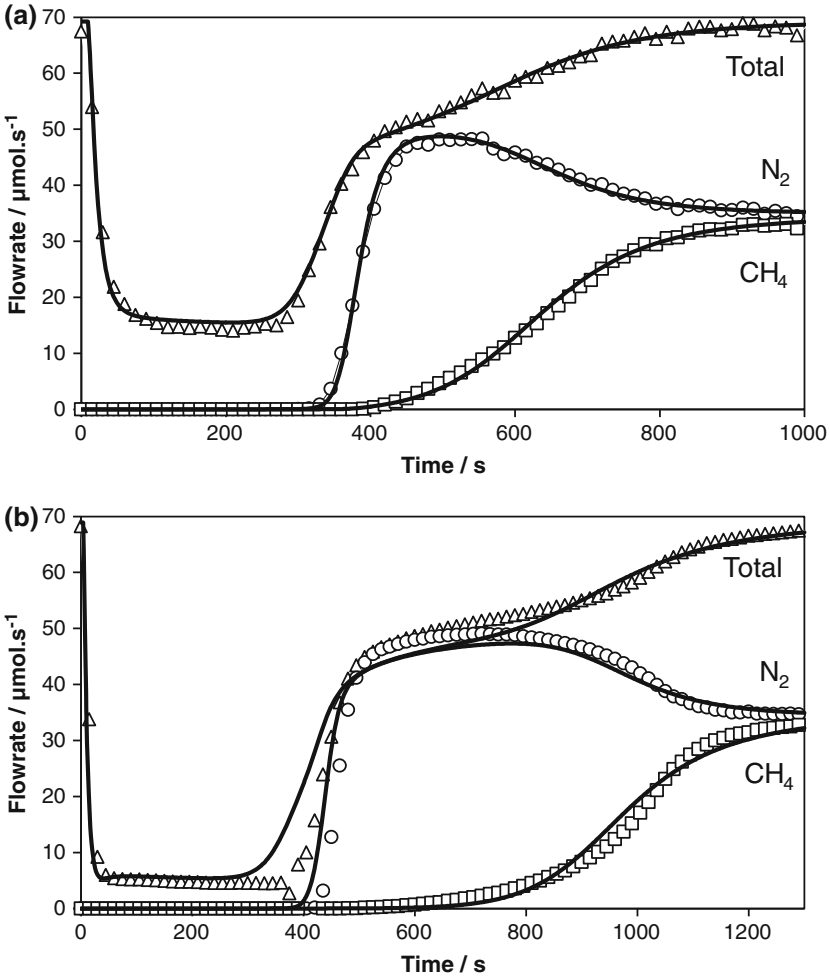

Fig. 8 Measured and predicted breakthroughs of an equimolar N_2:CH_4 gas mixture. **a** Best prediction with a r.m.s.d. of 0.8 µmol s^{-1} (304.0 kPa, 302.9 K). **b** Worst prediction with a r.m.s.d. of 2.9 µmol s^{-1} (107.8 kPa, 243.6 K). Experimental data were collected at 1 s intervals with not all points shown here

breakthrough experiment and (ii) its occurrence near the end of the experiment after the majority of the adsorption has occurred.

5 Breakthrough predictions for binary adsorbate mixtures and conclusions

Breakthrough curves for the DCB experiments with equimolar $CH_4 + N_2$ mixtures were predicted using the Extended Langmuir model (Eq. (1)) and the MTC_i values of CH_4 and N_2 predicted by the linear correlations shown in Fig. 6. Figure 8 shows two such comparisons for the cases in which the predicted flows had (a) the smallest and (b) the largest r.m.s. deviations from the measured flows, which occurred at the conditions 304.0 kPa, 302.9 K and 107.8 kPa, 243.6 K, respectively. The average r.m.s. deviation of the predictions from the observed data was 1.9 µmol s^{-1}, which is approximately 4 % of the average experimental flow rate. It can be seen in Figure 8 that, even in the worst case, the model produces a reasonable

Table 7 Root mean square deviations between measured and predicted breakthrough flow data for equimolar mixtures of CH_4 and N_2

Pressure (kPa)	Temperature (K)	r.m.s.d. (µmol s^{-1})
106.0	302.9	2.0
304.0	302.9	0.8
503.1	302.9	1.1
703.0	302.9	1.4
902.2	302.9	2.1
105.8	282.9	2.0
502.7	282.9	1.3
901.7	282.9	2.1
107.4	263.0	2.1
503.2	263.0	1.3
902.0	263.0	2.3
107.8	243.6	2.9
303.4	243.7	2.5
503.2	243.6	1.6
702.5	243.7	2.7
902.4	243.6	2.4

prediction of the observed data with an r.m.s. deviation of 2.9 μmol s^{-1}. Table 7 provides a summary of the comparisons of model predictions and experimental data.

In this work we have presented capacity and kinetic measurements of the adsorption of CH_4 and N_2 on H^+-mordenite using a DCB apparatus with (concentrated) pure gases and gas mixtures. The work demonstrated that dynamic gas mixture separations can be predicted reliably using correlations for the capacities and MTCs of pure fluids. The Extended Langmuir model for these adsorbates gave adequate mixture capacity predictions in comparison with the IAST, which is important given the computational efficiencies required to simulate both DCB experiments and PSA cycles with mixtures.

A numerical model of the DCB was used to extract MTCs for CH_4 and N_2 from the measured breakthrough curves. The model assumed that the adsorption rate was described by the LDF approximation with a lumped MTC. All parameters in the model, apart from the MTC, were fixed during the regression to limit the significant effect of parameter correlation. The pure fluid kinetic parameters were correlated with temperature and pressure, as shown in Figure 6, and used successfully to predict the breakthroughs observed in experiments with binary adsorbate mixtures.

The MTCs measured at pressures less than 110 kPa were outliers relative to the data measured at higher pressures. This was caused by an apparatus systematic error associated with the hold-up of helium in the mass spectrometer. Future work with this apparatus will address this limitation, as well as investigate the variation of the MTC with gas velocity and gas concentration (e.g. conduct dilute experiments with helium at the same total pressure).

Acknowledgments The research was funded by Chevron Energy Technology Company, the Western Australian Energy Research Alliance and the Australian Research Council (Project LP0776928). We thank Craig Grimm for helping to construct the apparatus, as well as David Zhang for his contribution to the research.

References

Ackley, M.W., Yang, R.T.: Kinetic separation by pressure swing adsorption—method of characteristics model. AIChE J. **36**(8), 1229–1238 (1990)

American Energies Pipeline, LLC: Improve Gas Quality-Nitrogen Rejection Unit. http://www.nitrogenrejectionunit.com (2011). Accessed 29 Oct 2010

Baker, R.W.: Future directions of membrane gas separation technology. Ind. Eng. Chem. Res. **41**, 1393–1411 (2002)

Bevington, P.R., Robinson, D.K.: Data Reduction and Error Analysis for the Physical Sciences. McGraw-Hill, Boston (1992)

Bird, R.B., Stewart, W.E., Lightfoot, E.N.: Transport Phenomena, 2nd edn. Wiley International, New York (2002)

Casas, N., Schell, J., Pini, R., Mazzotti, M.: Fixed bed adsorption of CO_2/H_2 mixtures on activated carbon: experiments and modeling. Adsorption **18**(2), 143–161 (2012). doi:10.1007/s10450-012-9389-z

Cavenati, S., Grande, C.A., Rodrigues, A.: Separation of $CH_4/CO_2/N_2$ mixtures by layered pressure swing adsorption for upgrade of natural gas. Chem. Eng. Sci. **61**, 3893–3906 (2006)

Churchill, S.W., Bernstein, M.: Correlating equation for forced-convection from gases and liquids to a circular-cylinder in cross-flow. J. Heat Transf. **99**(2), 300–306 (1977)

Delgado, J.: A critical review of dispersion in packed beds. Heat Mass Transf. **42**, 279–310 (2006). doi:10.1007/s00231-005-0019-0

Delgado, J.A., Uguina, M.A., Gomez, J.M., Ortega, L.: Adsorption equilibrium of carbon dioxide, methane and nitrogen onto Na- and H-mordenite at high pressures. Sep. Purif. Technol. **48**(3), 223–228 (2006a). doi:10.1016/j.seppur.2005.07.027

Delgado, J.A., Uguina, M.A., Sotelo, J.L., Ruiz, B.: Modelling of the fixed-bed adsorption of methane/nitrogen mixtures on silicalite pellets. Sep. Purif. Technol. **50**(2), 192–203 (2006b). doi:10.1016/j.seppur.2005.11.026

Guntuka, S., Farooq, S., Rajendran, A.: A- and B-Site substituted lanthanum cobaltite perovskite as high temperature oxygen sorbent. 2. Column dynamics study. Ind. Eng. Chem. Res. **47**(1), 163–170 (2008). doi:10.1021/ie070860p

Hofman, P.S., Rufford, T.E., Chan, K.I., May, E.F.: A dynamic column breakthrough apparatus for adsorption capacity measurements with quantitative uncertainties. Adsorption **18**(3–4), 251–263 (2012). doi:10.1007/s10450-012-9398-y

Jayaraman, A., Hernández-Maldonado, A.J., Yang, R.T., Chinn, D., Munson, C.L., Mohr, D.H.: Clinoptilolites for nitrogen/methane separation. Chem. Eng. Sci. **59**, 2407–2417 (2004)

Jensen, N.K., Rufford, T.E., Watson, G.C.Y., Zhang, D., Chan, K.I., May, E.F.: Screening zeolites for gas separation applications involving methane, nitrogen, and carbon dioxide. J. Chem. Eng. Data **57**(1), 106–113 (2012). doi:10.1021/je200817w

Kast, W.: Adsorption aus der gasphase—ingenieurwissenschaftliche Grundlagen und technische verfahren. VCH, Weinheim (1988)

Kidnay, A.J., Parrish, W.: Fundamentals of Natural Gas Processing. CRC Press, Boca Raton (2006)

Kunz, O., Klimeck, R., Wagner, W., Jaeschke, M.: The GERG-2004 Wide-Range Reference Equation of State for Natural Gases and Other Mixtures. GERG Technical Monograph. In. Fortschr.-Ber. VDI, VDI-Verlag, Düsseldorf (Germany), (2006)

Kuznicki, S.M., Bell, V.A., Petrovic, I., Blosser, P.W.: Separation of nitrogen from mixtures thereof with methane utilizing barium exchanged ETS-4. US Patent 5,989,316 (1999)

Lanfrey, P.Y., Kuzeljevic, Z.V., Dudukovic, M.P.: Tortuosity model for fixed beds randomly packed with identical particles. Chem. Eng. Sci. **65**(5), 1891–1896 (2010). doi:10.1016/j.ces.2009.11.011

Lemmon, E.W., Huber, M.L., McLinden, M.O.: REFPROP—Reference Fluid Thermodynamic and Transport Properties. NIST Standard Reference Database 23 (2007)

Malbrunot, P., Vidal, D., Vermesse, J., Chahine, R., Bose, T.K.: Adsorbent helium density measurement and its effect on adsorption isotherms at high pressure. Langmuir **13**, 539–544 (1997)

Malek, A., Farooq, S.: Determination of equilibrium isotherms using dynamic column breakthrough and constant flow equilibrium desorption. J. Chem. Eng. Data **41**(1), 25–32 (1996)

Mitariten, M.: Nitrogen removal from natural gas with the molecular gate™ adsorption process. In: 88th Annual Convention of the Gas Processors Association 2009, San Antonio, TX, 8–11 March 2009, pp. 544–555. Gas Processors Association

Mohamed, M.M.: Heat capacities, phase transitions and structural properties of cation-exchanged H-mordenite zeolites. Thermochim. Acta **372**(1–2), 75–83 (2001)

Mulgundmath, V.P., Jones, R.A., Tezel, F.H., Thibault, J.: Fixed bed adsorption for the removal of carbon dioxide from nitrogen:

breakthrough behaviour and modelling for heat and mass transfer. Sep. Purif. Technol. **85**, 17–27 (2012)

Myers, A.L., Prausnitz, J.M.: Thermodynamics of mixed-gas adsorption. AIChE J. **11**, 121–127 (1965)

Puértolas, B., Navarro, M.V., Lopez, J.M., Murillo, R., Mastral, A.M., Garcia, T.: Modelling the heat and mass transfer of propane onto a ZSM-5 zeolite. Sep. Purif. Technol. **86**, 127–136 (2012)

Rajendran, A., Kariwala, V., Farooq, S.: Correction procedures for extra-column effects in dynamic column breakthrough experiments. Chem. Eng. Sci. **63**(10), 2696–2706 (2008). doi:10.1016/j.ces.2008.02.023

Reid, R.C., Prausnitz, J.M., Poling, B.E.: The Properties of Gases and Liquids, 4th edn. McGraw-Hill, New York (1987)

Schiesser, W.E.: The Numerical Method of Lines. Academic Press, San Diego (1991)

Simo, M., Brown, C.J., Hlavacek, V.: Simulation of pressure swing adsorption in fuel ethanol production process. Comput. Chem. Eng. **32**(7), 1635–1649 (2008). doi:10.1016/j.compchemeng.2007.07.011

Sircar, S.: Basic research needs for design of adsorptive gas separation processes. Ind. Eng. Chem. Res. **45**(16), 5435–5448 (2006). doi:10.1021/ie051056a

Sircar, S., Hufton, J.R.: Why does the linear driving force model for adsorption kinetics work? Adsorption **6**(2), 137–147 (2000). doi:10.1023/A:1008965317983

Sudibandriyo, M., Pan, Z., Fitzgerald, J.E., Robinson, R.L., Gasem, K.A.M.: Adsorption of methane, nitrogen, carbon dioxide, and their binary mixtures on dry activated carbon at 318.2 K and pressures up to 13.6 MPa. Langmuir **19**(13), 5323–5331 (2003). doi:10.1021/la020976k

Valenzuela, D.P., Myers, A.L.: Adsorption Equilibrium Data Handbook. Advanced Reference Series. Prentice Hall, Englewood Cliffs (1989)

Warmuzinski, K., Tanczyk, M.: Multicomponent pressure swing adsorption. 1. Modelling of large-scale PSA installations. Chem. Eng. Process. **36**(2), 89–99 (1997)

Watson, G., May, E.F., Graham, B.F., Trebble, M.A., Trengove, R.D., Chan, K.I.: Equilibrium adsorption measurement of pure nitrogen, carbon dioxide, and methane on a carbon molecular sieve at cryogenic temperatures and high pressures. J. Chem. Eng. Data **54**, 2701–2707 (2009). doi:10.1021/je900224w

Yang, R.T.: Gas Separation by Adsorption Processes. Series on Chemical Engineering, vol. 1. World Scientific, Singapore (1997)